Plasma fluorination of diamond-like carbon surfaces: mechanism and application to nanoimprint lithography

2009 Nanotechnology 20 145306

(http://iopscience.iop.org/0957-4484/20/14/145306)

Nanotechnology **20** (2009) 145306 (7pp) doi:10.1088/0957-4484/20/14/145306

Plasma fluorination of diamond-like carbon surfaces: mechanism and application to nanoimprint lithography

M Schvartzman[1] **and S J Wind**[2]

[1] Department of Chemical Engineering, Columbia University, New York, NY 10027, USA
[2] Department of Applied Physics and Applied Mathematics, Columbia University, New York, NY 10027, USA

E-mail: sw2128@columbia.edu

Received 23 December 2008, in final form 19 February 2009
Published 17 March 2009
Online at stacks.iop.org/Nano/20/145306

Abstract

Diamond-like carbon (DLC) films, used as molds for nanoimprint lithography, were treated with a fluorocarbon-based plasma in order to enhance their anti-adhesion properties. While ellipsometry and atomic force microscope measurements showed negligible changes in thickness and surface roughness after plasma processing, contact angle measurement found fluorine plasma-treated DLC surfaces to be highly hydrophobic, with surface energy values reduced from ∼45 mJ m^{-2} for untreated films to ∼20–30 mJ m^{-2} after fluorination. X-ray photoelectron spectroscopy revealed a thin (from ∼0.5 to ∼3 nm) fluorocarbon layer on the DLC surface. Proposed mechanisms for the formation of this layer include two competing processes: etching of DLC and deposition of fluorocarbon material, with one or the other mechanism dominant, depending on the plasma conditions. Fluorocarbon plasma-treated DLC molds for nanoimprint lithography were used to pattern sub-20 nm size features with a high degree of repeatability, demonstrating an extended lifetime of the anti-adhesion coating.

(Some figures in this article are in colour only in the electronic version)

1. Introduction

Diamond-like carbon (DLC) is a widely used material for anti-wear and anti-adhesion applications due to its high mechanical strength [1]. It is a mildly hydrophobic material with a contact angle for water in air in the range of 60°–80° [2, 3] depending on synthesis and measurement methods. For some applications, however, its surface energy is found to be too high, prompting the need for additional surface treatment to lower its surface energy and to increase its hydrophobicity.

The mechanical properties of DLC make it an intriguing material for use as a mold in nanoimprint lithography (NIL), a technique which was introduced more than a decade ago as a cheap, high throughput process for ultra-small pattern definition [4]. Most of the recent developments in this technology have focused on materials engineering related either to the imprint polymer [5, 6] or to the mold [7]. In general, the NIL mold should meet three key materials-related requirements: (1) it should be compatible with the existing nanofabrication process; (2) it should have sufficient mechanical strength, which will make the mold resistant to the high pressure applied during the imprint and prevent its failure; and (3) it should have sufficient anti-adhesion properties for clear and easy mold–substrate separation at the end of the imprint process. Silicon dioxide and quartz are the most widely used materials for nanoimprint molds, while the anti-adhesive properties of the mold surface are usually achieved by the deposition of an organic self-assembled monolayer (SAM) with fluorinated outer functional groups. This is generally done by immersing the mold into a solution containing the release agent [8] or by vapor deposition [9]. It has been found, however, that these SAM release layers do not always work well for molds with sub-100 nm pitch with high aspect ratios [10], possibly because of imperfect assembly on nanoscale topographies. In addition, these coatings can degrade after a number of imprints [11], requiring reapplication of the coating to enable further use of the same mold.

The use of DLC films as a mold material for NIL was introduced about 2 years ago by Ramachandran *et al* [12]. They reported that successful mold release was obtained when pure CF_4 gas was used for reactive ion etching (RIE) of the DLC as a part of the mold fabrication process, which probably results in the presence of fluoro-organic species on the surface. Such anti-adhesion characteristics were not obtained when oxygen was added to the reactant gas mixture. Bulk fluorination of DLC for NIL mold application can be used to lower its surface energy as well [13], but this may result in compromise of the mold mechanical properties [14]. In a similar work, Nakamatsu *et al* [15] used a 50 nm-thick fluorinated DLC film as an anti-sticking coating for Si/SiO_2-based molds for the patterning of 200 nm features by NIL.

While fluorinated DLC has been shown to possess good anti-adhesion properties suitable for applications such as NIL, conditions under which it can be generally used for ultra-high resolution (i.e., less than ∼20 nm) patterning have not yet been demonstrated. Such applications require an extremely thin anti-adhesion layer which will not detract from the resolution of the original mold patterning. An appropriate process for forming such layers on patterned molds is required, and the properties of these layers should be properly studied. In our paper we characterize the process of fluorocarbon plasma treatment of DLC surfaces, which was demonstrated as feasible for achieving an anti-adhesion coating for NIL [16]. DLC films of ∼100 nm thickness deposited on Si substrates were used to study plasma fluorination under a range of process parameters such as chamber pressure and RF power, using either C_4F_8 or CHF_3 as source gases. Various surface analytical techniques were used in order to develop a fundamental understanding of the chemical and physical changes to the DLC surface as a result of plasma fluorination. The NIL mold fabrication process itself (described below) was simplified by choosing a masking material which is impervious to the etching of the DLC in an O_2 plasma, a step which precedes the DLC fluorination. These processes were then applied to NIL molds which were used to pattern features with sub-20 nm dimensions.

2. Experimental details

2.1. DLC film deposition

The DLC films were deposited in a parallel plate RF PECVD reactor with the substrate electrode powered by the RF. Films were deposited by first sputter etching the silicon wafer in an Ar plasma at 100 mTorr and 125 W for 30 s. The DLC was deposited using pure cyclohexane at 100 mTorr and 200 W. Under these conditions the growth rate of DLC is 3.4 nm s^{-1}. Total film thicknesses were 100 and 200 nm.

2.2. DLC surface fluorination

Fluorination was done in an Oxford PlasmaLab 80 Plus etcher at room temperature, using C_4F_8 and CHF_3 gases, chamber pressure in the range of 33–88 mTorr, gas flow rate of 100 sccm and RF power in the range of 100–300 W. Plasma fluorination time was 30 s for all samples.

2.3. Characterization of treated surfaces

The DLC layer thickness before and after fluorination was measured using a Rudolf El III null ellipsometer. Advancing contact angle measurements of water and glycerol were performed using a model 100-00 contact angle goniometer (Rame-Hart, Inc.)

AFM (PSIA XE-100) in tapping mode was used for the surface roughness measurements.

XPS analysis of the fluorinated and untreated DLC surfaces was performed in a Kratos Axis Ultra spectrometer using an Al Kα 1486 eV monochromatic x-ray source. Area of analysis was 700 μm × 300 μm in size. Survey (low resolution wide scan) was acquired at 80 eV pass energy. High resolution C 1s, F 1s and O 1s spectra were acquired at 20 eV pass energy. Three take-off-angles were used: 0°, 40° and 70°. Linear background was used for quantification of C 1s, O 1s and F 1s spectra. C 1s spectra were curve-fit using a mixture of Gaussian/Lorentzian peaks.

2.4. Mold fabrication and nanoimprint

1 cm^2 substrates were used for the mold preparation. Patterning was done using an FEI XL 30 Sirion scanning electron microscope equipped with a Nabity NPGS pattern generator. Exposure was done at 30 keV with a probe current of 25 pA for the highest resolution features. A 20 nm-thick film of hydrogen silsesquioxane (FOx-12, Dow Corning), diluted in MIBK, was applied on the substrate by spin coating. No post-baking was used in order to maximize contrast [17]. The pattern consisted of single-pixel dots, arranged either in rectangular arrays with the period of 100 nm, or, alternatively, in arrays of pairs of dots separated by 40–100 nm, with a constant spacing of 200 nm between the pairs. Each array extended over an area a few microns in size. A range of point exposure doses (from 7 to 18 fC) were used in order to obtain different dot diameters. The samples were developed in Microposit™ LDD(TM)—26W Developer (Rohm and Haas Electronic Materials). The pattern transfer to the DLC layer was done by O_2 RIE using an Oxford PlasmaLab 80 Plus ICP system, resulting in 50 nm-tall pillars. The high etch selectivity of DLC to HSQ in oxygen plasma allowed us to use a relatively thin HSQ mask, without any additional hard masking material. A C_4F_8 plasma process was applied afterward for 30 s, typically using 88 mTorr chamber pressure and 100 W power as process parameters. Finally, HSQ mask residuals were removed by a short dip (10 s) in a buffered oxide etch solution and DI water rinse.

Thermal nanoimprint was done using a Nanonex BX-200 nanoimprinter. PMMA (25 K) diluted in anisole was applied on Si substrates by spin coating, and baked on a hot plate at 180 °C for 5 min. The nanoimprint process was done at a temperature of 175 °C and a pressure of 26 kTorr. The imprint time was 5 min.

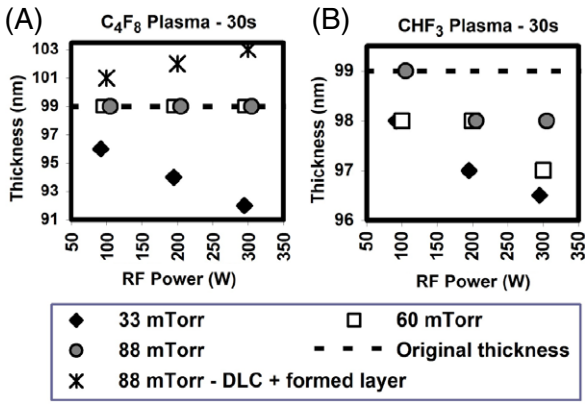

Figure 1. DLC thickness for (A) C_4F_8 and (B) CHF_3 plasma treatments as a function of RF power for several values of chamber pressure. The original thickness of the DLC film was 99 nm.

3. Experimental results

3.1. Fluorinated DLC thickness

The fluorinated plasma surface treatment was applied on Si substrates (1 cm × 1 cm) covered with 99 nm-thick DLC films, and the change in DLC thickness was monitored by null ellipsometry. The following conditions were used for the plasma process: chamber pressure in the range of 33–88 mTorr, RF power in the range of 100–300 W, gas flow rate of 100 sccm and a process time of 30 s. For most of the conditions, a slight reduction in the DLC thickness upon plasma fluorination was observed. The DLC thickness for samples exposed to C_4F_8 and CHF_3 plasmas is shown in figure 1. Under most of the conditions studied, the DLC was etched to a depth up to a few nm. However, for samples treated by C_4F_8 at a pressure of 88 mTorr, a layer of thickness ∼1–3 nm with a refractive index of 1.48 (at 632.8 nm wavelength) was detected at the top of the DLC film, while the original DLC thickness remained unchanged.

3.2. Contact angle measurements

Figure 2 shows the change in the advancing contact angle of water and glycerol (respectively) following plasma treatment with C_4F_8 and CHF_3, as a function of chamber pressure and RF power. These results are to be compared with those obtained for a Si/SiO_2 substrate coated with a commercial monolayer mold release agent NXT-110-A® (Nanonex), whose contact angle was 87° for water and 78° for glycerol.

Surface energies (γ_S), as well as their polar and dispersive components (γ_S^p and γ_S^d respectively) were calculated based on the contact angle data. Two different methods were used for these calculations. The two-liquid geometric method [18, 19] uses the following form for the dependence of the of the contact angle on the polar and dispersive components of both liquid and solid surface energies:

$$1 + \cos\theta = 2\sqrt{\gamma_S^d}\left(\frac{\sqrt{\gamma_{LV}^d}}{\gamma_{LV}}\right) + 2\sqrt{\gamma_S^p}\left(\frac{\sqrt{\gamma_{LV}^p}}{\gamma_{LV}}\right) \qquad (1)$$

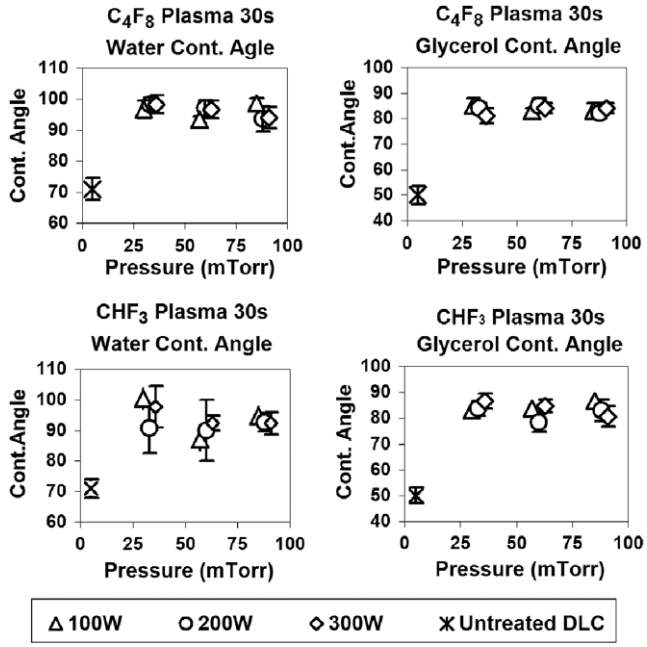

Figure 2. Water contact angle of C_4F_8 and CHF_3 plasma-treated DLC surfaces.

where γ_L, γ_L^p and γ_L^d are the free energy of the liquid against its saturated vapor, and its polar and dispersive components respectively. γ_S, γ_S^p and γ_S^d can be calculated by solving a system of two equations—one for each liquid.

The two-liquid harmonic method [20] provides an alternative method for the surface energy calculation, by solving a system of two equations (each one for each liquid) of the following type:

$$1 + \cos\theta = \frac{1}{\gamma_{LV}}\left(\frac{4\gamma_S^d\gamma_{LV}^d}{\gamma_S^d + \gamma_{LV}^d} - \frac{4\gamma_S^p\gamma_{LV}^p}{\gamma_S^p + \gamma_{LV}^p}\right). \qquad (2)$$

The results of the surface energy calculations are shown in figure 3. The values of the polar and dispersive surface energy was $\gamma_L^p = 51.0$ mJ m^{-2} and $\gamma_L^d = 21.8$ mJ m^{-2} for water and $\gamma_L^p = 26.4$ mJ m^{-2} and $\gamma_L^d = 37.0$ mJ m^{-2} for glycerol, respectively [21]. In general, the surface energy values as calculated by the harmonic method were 2–3 mJ m^{-2} higher than those calculated by the geometric method.

3.3. XPS analysis

XPS was used to analyze the surface chemical composition of DLC samples treated with C_4F_8 plasma under three different sets of conditions: 33 mTorr, 200 W (sample 1); 60 mTorr, 200 W (sample 2); and 88 mTorr, 200 W (sample 3), as well as for an untreated DLC film. Table 1 shows the elemental quantification of the samples derived from the XPS measurements; the analysis was done for depths from 2 to 9 nm.

The data show clear evidence for the presence of fluorine at the surface of the treated samples, probably as a part of a fluorocarbon compound. The carbon/fluorine ratio was calculated from the elemental quantification data for every sample versus measured depth (figure 4).

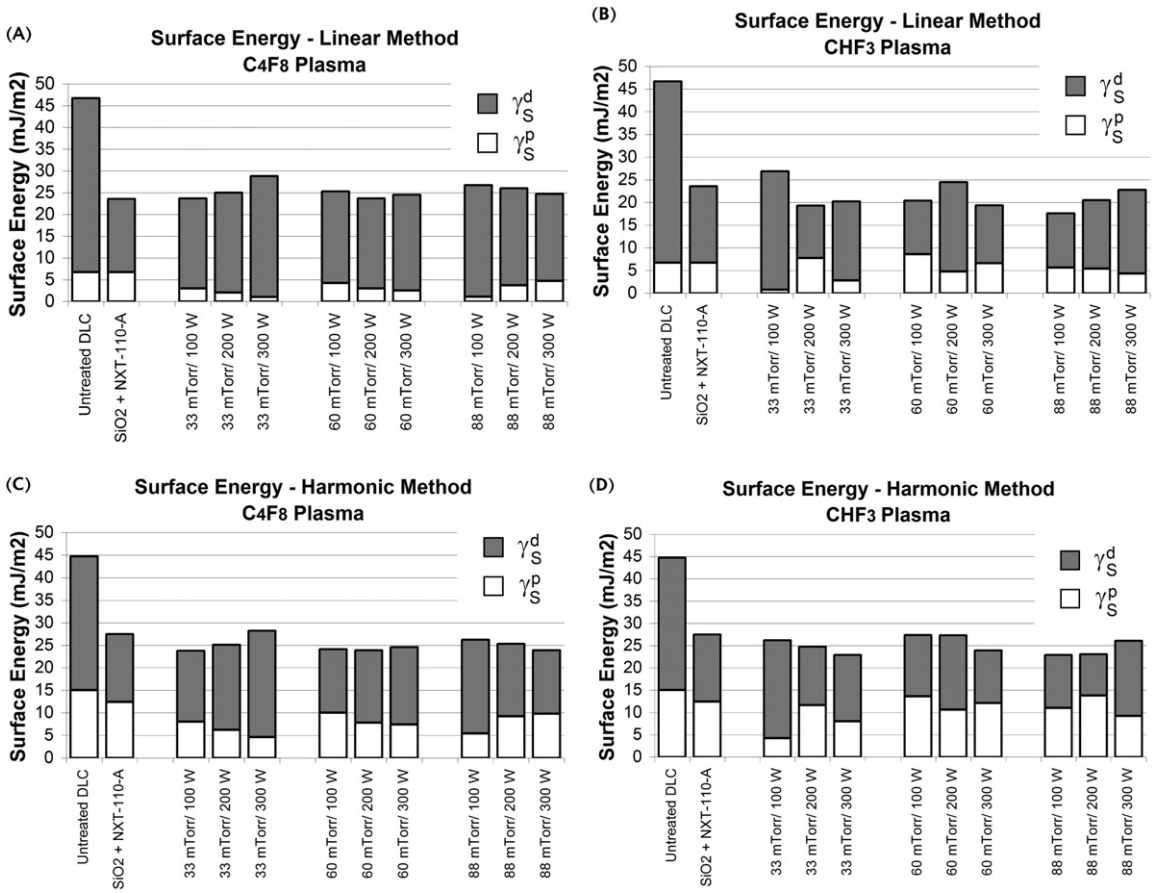

Figure 3. Surface energy and its polar (γ_S^p) and dispersive (γ_S^d) components as a function of plasma fluorination parameters for DLC surfaces treated in C_4F_8 ((A), (C)) and CHF_3 ((B), (D)) plasma. Each plot also shows the surface energy values calculated for untreated DLC and SiO_2 surface treated with NXT-110-A® (Nanonex) mold release agent.

Table 1. XPS—elemental quantification.

	DLC		Sample 1			Sample 2			Sample 3		
Depth (nm)	C 1s (%)	O 1s (%)	C 1s (%)	F 1s (%)	O 1s (%)	C 1s (%)	F 1s (%)	O 1s (%)	C 1s (%)	F 1s (%)	O 1s (%)
2–3	88.4	11.6	53.3	44.2	2.5	49	48.4	2.6	40.6	58.1	1.2
5–7	89.1	10.9	60.1	37.7	2.1	53	44.1	2.9	38.6	60.1	1.2
6–9	89.4	10.6	61	36.9	2.1	54.2	42.9	2.9	36	62.3	1.6

It can be seen from figure 4 that for samples 1 and 2 the relative amount of carbon increases with increasing depth, suggesting the existence of a very thin fluorine-containing layer at the surface, with a thickness not greater than ∼1–2 nm. The nearly constant C/F ratio (with a slight decrease) for sample 3 can be explained by a thicker fluorine-contained layer as compared to samples 1 and 2.

The XPS data were deconvolved in order to identify different carbon functional groups (figure 5). For C 1s deconvolution of peaks, DLC was curve-fit using asymmetric G/L peak specific to graphitic character. Small amounts of C–O species were detected. The same peak was used in the plasma-modified samples. Five peaks in addition to graphitic carbon were detected in fluorinated samples—due to C–F, CF_2, CF_3, secondary shift C*–CF and C=O species. For samples 1 and 2, a significant amount of graphitic carbon was observed and it decreased at lower depth. The largest peak among those formed as a result of plasma treatment is the one due to C–F. For sample 3, almost no graphitic carbon was observed. The largest peaks were those due to $CF_2 > CF > CF_3$. There was more of C–F species towards the surface, while the CF_2 peaks were evenly distributed.

The thicknesses of the fluorine-containing layers was determined from the data collected from 3 take-off-angle measurements: 0°, 40° and 70°, using the value of the mean free path of diamond for DLC (table 2).

3.4. AFM analysis

The surface roughness of the DLC film was measured by atomic force microscopy (tapping mode). The surface roughness of untreated DLC films had a RMS value of 0.72 nm.

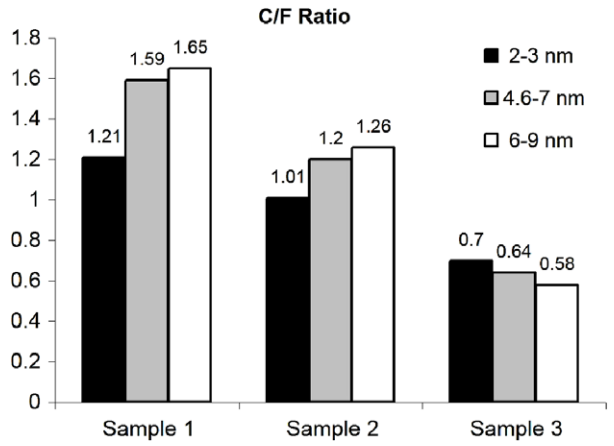

Figure 4. Integrated C/F ratio at different depths.

Oxygen plasma etching was found to reduce the roughness RMS to 0.18 nm. A standard fluorination process, used for nanoimprint mold fabrication (C_2F_6 plasma, 88 mTorr, RF power = 100 W), increased the roughness of the O_2 etched DLC to 0.45 nm (figure 6).

3.5. Nanoimprint lithography

DLC films were patterned by electron beam lithography using a negative tone resist (hydrogen silsesquioxane, or HSQ). The pattern consisted of features with different shapes and sizes ranging from a few tens of microns down to ∼15 nm. The pattern was transferred into the DLC film by O_2 plasma etching, followed *in situ* plasma fluorination and residual HSQ strip, resulting in features with a height of 30–50 nm (depending on the etching time), with the aspect ratio as high as ∼1:3 for the smallest ones. AFM scans of the patterned areas were used to confirm the feature height.

Table 2. Mean thicknesses of the fluorine-containing layers, calculated for DLC.

Sample	Mean thickness (nm)
1	0.51
2	0.72
3	2.84

The plasma fluorinated molds were used for thermal NIL in PMMA resist on Si substrates. After the mold–substrate separation, PMMA residue was usually observed on molds that did not undergo plasma fluorination. This residue is caused by detachment of PMMA from the imprinted surface, leaving defects in the pattern formed by NIL, as seen in figure 7(A). NIL using the fluorinated DLC molds resulted in clear and easy mold–substrate separation after the imprint, with no PMMA residue on the mold, and high quality pattern transfer from the mold to the PMMA-coated substrate, as seen in figure 7(B). The anti-adhesion coating provided by the plasma fluorination process withstood more than 100 imprints, with no change in the imprint quality. An SEM image of the imprinted PMMA in figure 8 shows a clear and reliable pattern transfer from the mold to the PMMA-coated substrate. In this case the pattern consisted of an array of dots ∼15 nm in diameter.

4. Discussion

Exposure to a fluorocarbon plasma without the addition of oxygen to the reactive gas flow usually results in formation of polymer-like fluorocarbon film on the surface [22]. Fluorocarbon film formation can easily explain the highly hydrophobic properties of the treated surfaces observed in our contact angle measurements. These results are similar to those reported by Butter *et al* for fluorocarbon plasma-modified DLC surfaces, with water contact angles in the

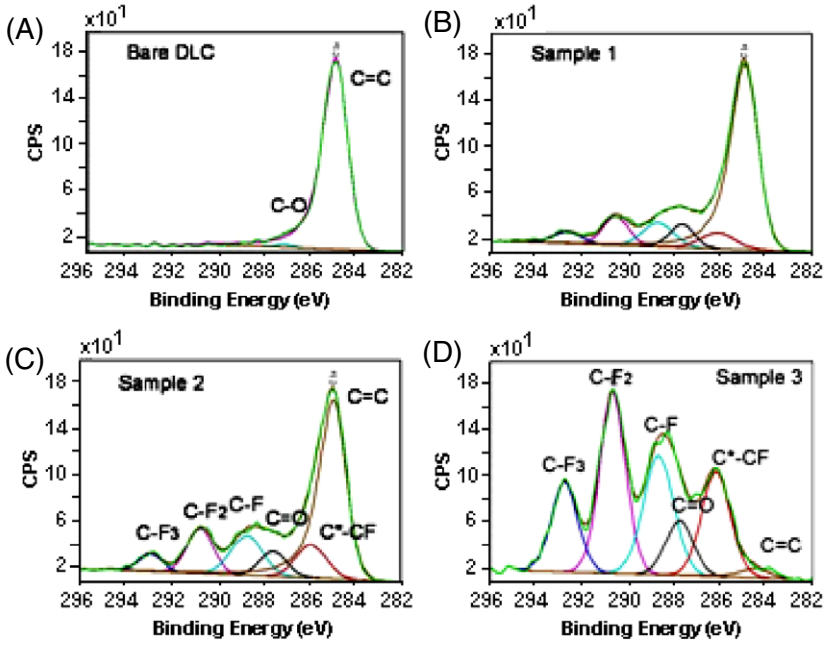

Figure 5. Deconvolution of XPS peaks.

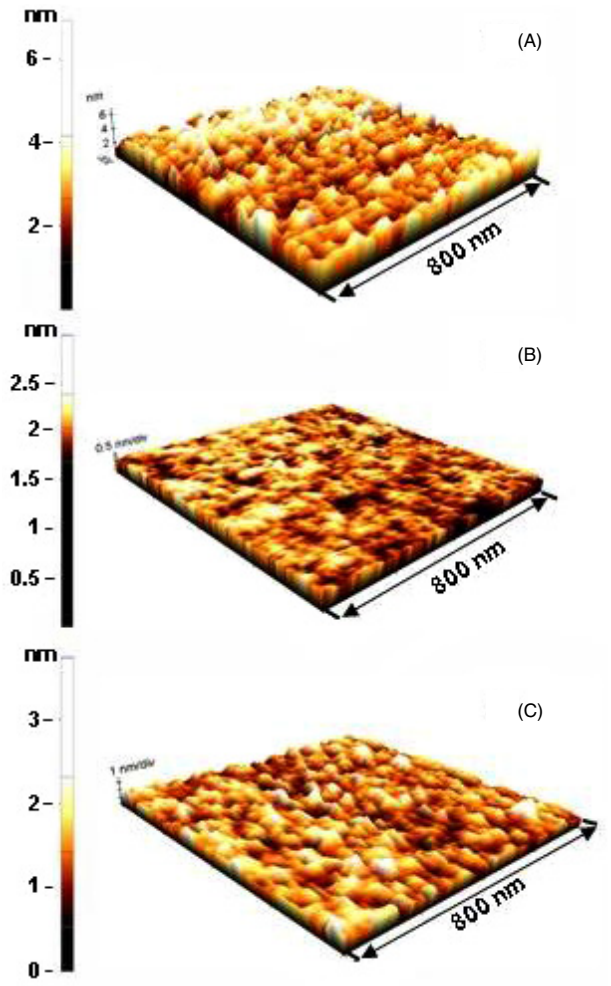

Figure 6. AFM images of the bare DLC film surface (A) after O_2 plasma etch and (B) after O_2 plasma etch followed by plasma fluorination.

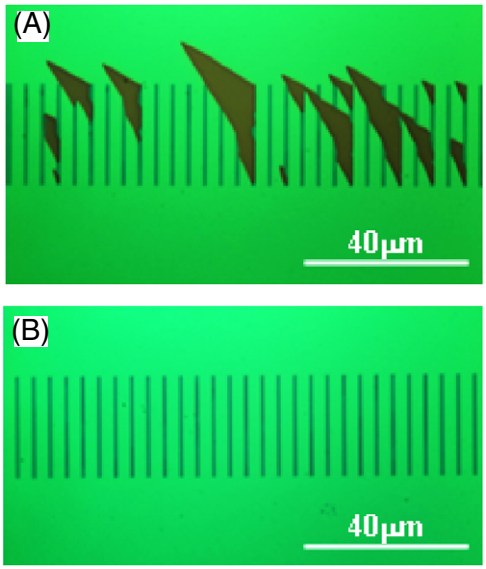

Figure 7. (A) NIL mold with an imperfect anti-wear coating after imprint. (B) Same type of mold with the fluorinated anti-wear coating after imprint.

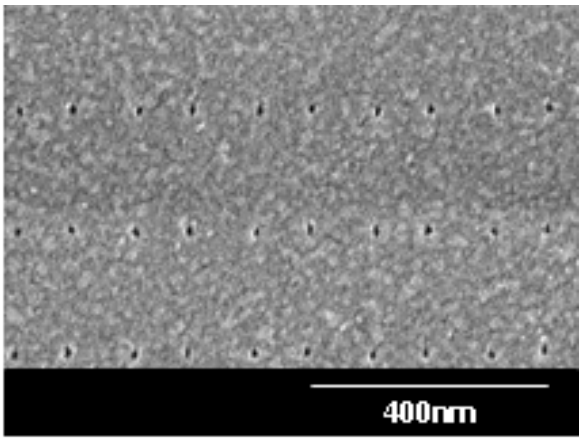

Figure 8. PMMA imprinted with the DLC mold.

range of 90°–110° [23]. In addition, our measured contact angles and calculated surface energies for the fluorinated DLC surfaces compare well to those of the SiO_2 treated with a commercial nanoimprint mold release agent, proving the efficacy of fluorinated DLC for NIL mold release. The surface energies measured for different fluorinated surfaces with values in the range of 23–28 mJ m^{-2} also compare well with those reported previously regarding fluorinated DLC surfaces [12, 23] and even to those of PTFE, for which γ_S is about 22 mJ m^{-2} [24]. Despite the similarity of the γ_S values to those of fluoropolymers and fluorocarbon-coated surfaces, it is difficult to explain its relatively high polar component, obtained both from the linear and harmonic two-liquids methods. We could not see any clear dependence of the wetting properties and the surface energies on the plasma process parameters. This is most likely due to the robustness of the fluorination process within the window of parameters studied.

Based on the XPS analysis of the C_4F_8 plasma-treated surfaces, it could be inferred that the anti-adhesion surface properties are due to the formation of a thin (from ∼0.5 nm to a few nm) layer of a fluorocarbon compound, with a chemical content very close to that of PTFE [25]. Two possible mechanisms are proposed for the formation of this fluorinated layer. The first mechanism is the incorporation of the fluorine ions *into* the bulk during DLC etching, which is easily observed using surface analysis techniques such as XPS [26]. The depth of fluorine incorporation depends critically on the process parameters of plasma fluorination, and in some cases can extend to ∼5 nm [27]. The second mechanism is the *deposition* of a fluorocarbon film from the plasma, with thickness, structure, chemical content and physical properties that may vary depending on the plasma chamber design and process parameters [28]. Both these mechanisms can act concurrently. They compete with one another, as can be inferred from the ellipsometry and XPS analysis. For the lower chamber pressure (33 mTorr) a reduction in the bulk DLC thickness can be clearly seen (figure 1). Furthermore, the DLC etch rate seems to increase with RF power, which is consistent with general plasma etching phenomena. The very thin fluorocarbon layer (0.51 nm) which was detected by XPS analysis was not seen in the ellipsometry measurements,

probably due to the limited resolution of the ellipsometer. The increase in the C/F ratio with depth confirms that for the lower chamber pressure process, fluorine is present only in the vicinity of the surface (less than 2 nm depth). This suggests that for the lower pressure process the etching mechanism dominates. On the other hand, for the higher chamber pressure process, where the DLC etching rate is much slower and even negligible, but the observed fluorocarbon layer is thicker, the deposition mechanism dominates the etching. The C/F ratio remains nearly constant with depth (from 2 nm to 6–9 nm); this can be explained by both the relatively thick fluorocarbon layer and the deeper fluorine atom penetration.

An additional perspective on the formation of the fluorocarbon layer can be obtained by adopting the mechanism proposed by Standaert *et al* for fluorocarbon plasma etching of Si [29]. According to that study, a thin (2–7 nm) fluorocarbon film is formed on the etched Si surface, and the etching occurs due to the diffusion of the fluorine species through the film into the bulk. This may occur in DLC etching as well, however, we have no direct evidence supporting this model in our case.

Fluorocarbon plasma treatment provides reliable anti-adhesion properties to the NIL mold surface. The imprinted PMMA surface remains clean and has no visible defects. The low surface energy results in weak adhesion of the PMMA to the mold in the mold–PMMA–imprinted substrate 'sandwich'. This adhesion is much weaker than that of the PMMA to the substrate (assuming that the substrate is clean and lacking defects) enabling easy post-NIL mold–substrate separation and leaving the mold clean of any PMMA residuals.

As mentioned above, DLC fabricated nanoimprint molds without any additional surface treatment gave poor results in terms of mold–substrate separation, and resulted in adhesion of PMMA to the mold surface. This leads to the conclusion that neither bare DLC (in spite of its well known anti-adhesion surface properties) nor DLC etched in an oxygen-containing plasma, is sufficiently hydrophobic for a good mold–substrate separation. This cannot be attributed to surface roughness, as AFM measurement indicates initially smooth surface of bare DLC with an RMS value of 0.72 nm with a further reduction to 0.18 nm following the O_2 RIE process.

5. Conclusions

Fluorination by fluorocarbon plasma was found to be an effective method for achieving anti-adhesion properties for DLC nanoimprint molds when applied at the end of the mold fabrication process. Wetting properties and surface energies were found to be comparable to those achieved by standard methods used by the nanoimprint community. Surface analysis showed a formation of a thin fluorocarbon film on the DLC surface responsible for these properties. Highly robust and reliable coating makes these molds well suited for high resolution nanoimprint lithography.

Acknowledgments

The authors thank Dr Christian Jahnes at the IBM T J Watson Research Center for providing DLC-coated substrates and Dr Kateryna Artyushkova at the University of New Mexico for assistance with XPS measurements and analysis. This work was supported by the National Institutes of Health through the NIH Roadmap for Medical Research under award number PN2EY016586 and by the National Science Foundation under award number NSF EF-05-07086. Additional support from the Nanoscale Science and Engineering Initiative of the National Science Foundation under NSF Award Number CHE-0641523 and by the New York State Office of Science, Technology, and Academic Research (NYSTAR) is also gratefully acknowledged.

References

[1] Robertson J 2002 *Mater. Sci. Eng.* R **37** 129
[2] Butter R S and Lettington A H 1994 New diamond and diamond-like films *Adv. Sci. Technol.* **6** 353
[3] Ohmac N and Tagawa M 2004 *Transient Processes in Tribology: Proc. 30th Leeds-Lyon Symp. on Tribiology* ed G Dalmaz
[4] Chou S Y, Krauss P R, Zhang W, Guo L and Zhuang L 1997 *J. Vac. Sci. Technol.* B **15** 2897
[5] Choi P, Fu P and Guo L J 2007 *Adv. Funct. Mater.* **17** 65
[6] Igaku Y, Matsui S, Ishigaku H, Fujita J, Ishida M, Ochiai Y, Namatsu H, Komuro M and Hiroshima H 2002 *Japan. J. Appl. Phys.* **41** 4198
[7] Guo L J 2007 *Adv. Mater.* **19** 495
[8] Junarsa I and Nealey P F 2004 *J. Vac. Sci. Technol.* B **22** 2685
[9] Zhang T, Kobrin B, Wanebo M, Nowak R, Yi R, Chinn J, Bender M, Fuchs A and Otto M 2006 Vapor deposited release layers for nanoimprint lithography *Proc. SPIE—Int. Soc. Opt. Eng.* **6151** 615117
[10] Jung G Y, Li Z Y, Wu W, Chen Y, Olynick D L, Wang S Y, Tong W M and Williams R S 2005 *Langmuir* **21** 1158
[11] Houle F A, Rettner C T, Miller D C and Sooriyakumaran R 2007 *Appl. Phys. Lett.* **90** 213103
[12] Ramachandran S, Tao L, Lee T H, Sant S, Overzet L J, Goeckner M J, Kim M J, Lee G S and Hu W 2006 *J. Vac. Sci. Technol.* B **24** 2993
[13] Altun A O, Jeong J H, Rha J J, Choi D G, Kim K D and Lee E S 2006 *Nanotechnology* **17** 4659
[14] Hakovirta M, Lee D H, He X M and Nastasi M 2001 *J. Vac. Sci. Technol.* A **19** 782
[15] Nakamatsu K, Yamada N, Kanda K, Haruyama Y and Matsui S 2006 *Japan. J. Appl. Phys.* **45** L954
[16] Schvartzman M, Mathur A, Hone J, Jahnes C and Wind S J 2008 *Appl. Phys. Lett.* **93** 153105
[17] Henschel W, Georgiev Y M and Kurz H 2003 *J. Vac. Sci. Technol.* B **21** 2018
[18] Kaelble D H and Uy K C 1970 *J. Adhes.* **2** 50
[19] Owens D K and Wendt R C 1969 *J. Appl. Polym. Sci.* **13** 1741
[20] Wu S 1971 *J. Polym. Sci.* C **34** 19
[21] Fowkes F M (ed) 1965 *Chemistry and Physics of Interfaces* (Washington, DC: American Chemical Society) chapter 1
[22] Standaert T E F M, Hedlund C, Joseph E A, Oehrlein G S and Dalton T J 2004 *J. Vac. Sci. Technol.* A **22** 53
[23] Butter R S, Waterman D R, Lettington A H, Ramos R T and Fordham E J 1997 *Thin Solid Films* **311** 107
[24] Dann J R 1970 *J. Colloid Interface Sci.* **32** 302
[25] Girardeaux C and Pireaux J J 1996 *Surf. Sci. Spectra* **4** 138
[26] Vivensang C, Turban G, Anger E and Gicquel A 1994 *Diamond Relat. Mater.* **3** 645
[27] Simko J P, Oehrlein G S and Mayer T M 1991 *J. Electrochem. Soc.* **138** 277
[28] D'Agostino R 1990 *Plasma Deposition, Treatment and Etching of Polymers* (New York: Academic) p 95
[29] Standaert T E F M, Schaepkens M, Rueger N R, Sebel P G M, Oehrlein G S and Cook J M 1998 *J. Vac. Sci. Technol.* A **16** 239